

The vulnerability of lakes to climate change along an altitudinal gradient

Love Råman Vinnå ^{1✉}, Iselin Medhaug ², Martin Schmid ¹ & Damien Bouffard ^{1✉}

Studies of future 21st century climate warming in lakes along altitudinal gradients have been partially obscured by local atmospheric phenomena unresolved in climate models. Here we forced the physical lake model Simstrat with locally downscaled climate models under three future scenarios to investigate the impact on 29 Swiss lakes, varying in size along an altitudinal gradient. Results from the worst-case scenario project substantial change at the end of the century in duration of ice-cover at mid to high altitude (−2 to −107 days), stratification duration (winter −17 to −84 days, summer −2 to 73 days), while lower and especially mid altitude (present day mean annual air temperature from 9 °C to 3 °C) dimictic lakes risk shift to monomictic regimes (seven out of the eight lakes). Analysis further indicates that for many lakes shifts in mixing regime can be avoided by adhering to the most stringent scenario.

¹Eawag, Swiss Federal Institute of Aquatic Science and Technology, Surface Waters—Research and Management, Kastanienbaum, Switzerland. ²Institute for Atmospheric and Climate Science, ETH Zürich, 8092 Zürich, Switzerland. ✉email: love.raman@hotmail.com; Damien.Bouffard@eawag.ch

Lakes are commonly cited as sentinels of climate change¹. The physical response of lakes to changes in atmospheric forcing are traditionally assessed by quantifying modifications in their thermal structure. These modifications typically include evolution of lake surface and bottom temperatures, the duration of the summer and winter stratification and the duration of ice cover. The mixing regime of lakes² is a physical parameter describing the timing and frequency with which lake temperatures fully homogenize on an annual basis. When compared with other physical characteristics, these events with homogenization of the water column exert the largest overall influence on the functioning of lake ecosystems. A change in mixing regime thus profoundly alters a lake by enhancing or preventing vertical fluxes of nutrients and dissolved gases. This in turn can reshape food web dynamics in the lake^{3–9}. Numerous studies have already reported specific effects of climate change on lake temperature^{10–12}, ice cover^{13–17}, stratification and mixing regime^{18–21} and nonlinear seasonal interactions²² at global and regional scales. These changes have been linked to trends in atmospheric climate variables (e.g. air temperature) and to individual lake characteristics (e.g. volume, area, transparency) either by statistical methods^{12,16,20,22,23} or process-based numerical models^{10,11,14,15,19,21,24,25}.

In addition to the well-studied latitudinal gradients in lake response to climatic change¹⁹, altitude-gradients in atmospheric conditions^{26,27} may also influence the thermal structure of lakes²⁸. Lake mixing regimes have classically been defined at global scales as a function of latitude and altitude². Given the altitude-dependence of both climate trends^{26,27} and lake mixing regimes², we hypothesize that lake response to climate change varies as a function of altitude. This hypothesis carries major implications for the vulnerability of lakes in terms of their ecosystems and their role in the carbon cycle. The remoteness of high altitude lakes however limits the availability of long-term datasets that might elucidate these relations^{26,29}. Given the lack of long-term data, modelling approaches can fill in gaps by estimating responses from past lake data and future projected climate scenarios. This study investigates altitude-dependencies on climate change by modelling the response of 29 lakes in Switzerland, spanning an altitudinal gradient from 193 to 1797 m a.s.l. (Fig. 1d and Table 1). The numerical simulations are performed with the deterministic one-dimensional physical lake model Simstrat^{30,31}.

An important challenge when modelling lakes along an altitudinal gradient is that the altitude-dependence of climate forcing in Regional Climate Model (RCM) projections is represented by averages over individual grid cells. The complex topography of mountainous areas can strongly affect local atmospheric conditions. In the present study, we address this challenge by using recently developed RCM projections downscaled to the local scale for Switzerland³². We specifically focus on the period from 1981 to 2099 using RCM projections for the three Representative Concentration Pathways (RCP), RCP8.5, RCP4.5 and RCP2.6 (Supplementary Fig. 1). The numbers at the end of the RCPs indicate the increased radiative forcing in W m^{-2} in the year 2100 compared to preindustrial levels. The worst-case scenario RCP8.5 implies continuously rising global greenhouse gas emissions, in RCP 4.5 emissions are peaking around 2050 and subsequently declining, while the most stringent scenario RCP2.6 was designed to limit global warming to 2°C in line with the Paris agreement and requires stringent measures for emission reduction and net negative emissions towards the end of the twenty-first century³³. Differences in climate between the late twenty-first century and the base period are here expressed as the median, mean and variance for 2071–2099 compared to 1982–2010.

The results of our simulations indicate that climate change will cause substantial alterations in the thermal structure of the 29 investigated lakes. Mean annual lake surface temperatures are

projected to consistently increase for all lakes. Projected changes in other thermal properties, such as lake bottom temperature and the duration of summer and winter stratification as well as ice cover, depend on individual lake properties such as lake volume and altitude. The projected changes in stratification and ice cover duration are largest for high altitude lakes. Nonetheless, these lakes will maintain their annual ice cover and a dimictic stratification regime throughout the twenty-first century. Low to mid altitude (<1500 m a.s.l.) small lakes (<0.5 km³) were found to be especially sensitive to changes. These lakes are projected to lose ice cover and change from a dimictic to a monomictic regime during the twenty-first century. Results based on different emission scenarios indicate that changes in mixing regime and loss of ice cover can be counteracted, but not entirely avoided, with climate protection measures as projected by scenario RCP2.6. The results of the present study cannot be directly transferred to other regions because the altitudinal variation of both lake thermal properties and trends in climate variables are not necessarily similar elsewhere. However, we would expect similar sensitivities of lakes to climate change in other regions where lake mixing regimes range from primarily monomictic at lower altitudes to dimictic at high altitudes. The investigations in the present study are limited to the direct impacts of projected changes in climate conditions on the thermal structure of lakes. Further investigations are needed to quantify possible indirect impacts, especially those resulting from changes in the lake catchments³⁴, including but not limited to glacier retreat and permafrost thaw³⁵, alterations of snow melt dynamics^{36,37}, river flow regimes and resulting changes in loads of suspended particles and nutrients^{38,39}. On a hopeful note, this study shows that many lakes can potentially avoid shifts in mixing regimes and sustain ice cover throughout the twenty-first century if greenhouse gas concentration trajectories remain within envelopes envisioned under RCP2.6.

Results and discussion

Altitudinal gradients in RCM forcing and heat fluxes. An analysis of the downscaled dataset confirmed altitude-dependent trends associated with several climate variables (Fig. 1). For RCP8.5, averaged air temperature trends across all RCM simulations are $\sim 20\%$ larger at 1700 m a.s.l. ($0.54^\circ\text{C decade}^{-1}$, Fig. 1c) than those at 450 m a.s.l. ($0.44^\circ\text{C decade}^{-1}$, Fig. 1a). Conversely, surface downward solar radiation (305–2800 nm) is projected to decrease at high altitudes ($-0.84 \text{ W m}^{-2} \text{ decade}^{-1}$ at 1700 m a.s.l. for RCP8.5, Fig. 1f) but not at low altitudes (Fig. 1d). Changes in shortwave solar radiation can in principle result from changes in cloud cover, in atmospheric water content, or in aerosol concentrations. A recent analysis showed that global climate models (GCMs) generally project significantly increasing surface downward shortwave radiation over Europe due to projected reduced anthropogenic aerosols⁴⁰. However, most EURO-CORDEX RCMs do not take into account the future evolution of these aerosols. The projected spatially variable shortwave radiation in these models, with decreasing radiation at high altitudes and latitudes (Fig. 1i, j) and increasing radiation elsewhere, is therefore likely related to the spatial variability in projected trends of cloud cover, cloud types and atmospheric water content in the RCM simulations. In the alpine region of Switzerland, this results in a significant negative altitudinal gradient of the solar radiation trend of $\sim -0.63 \text{ W m}^{-2} \text{ decade}^{-1} \text{ km}^{-1}$. For parts of the pre-alps, Jura Mountains and most mid to low altitudes (<1000 m a.s.l.) in south-west Europe, the RCMs show a positive trend for solar radiation (Fig. 1h–j). The projected wind speed reductions of ~ 0.003 (low altitude) to 0.008 (high altitude) $\text{m s}^{-1} \text{ decade}^{-1}$ for RCP8.5 are in line with historical observations for the alpine region but notably smaller than observed recent atmospheric

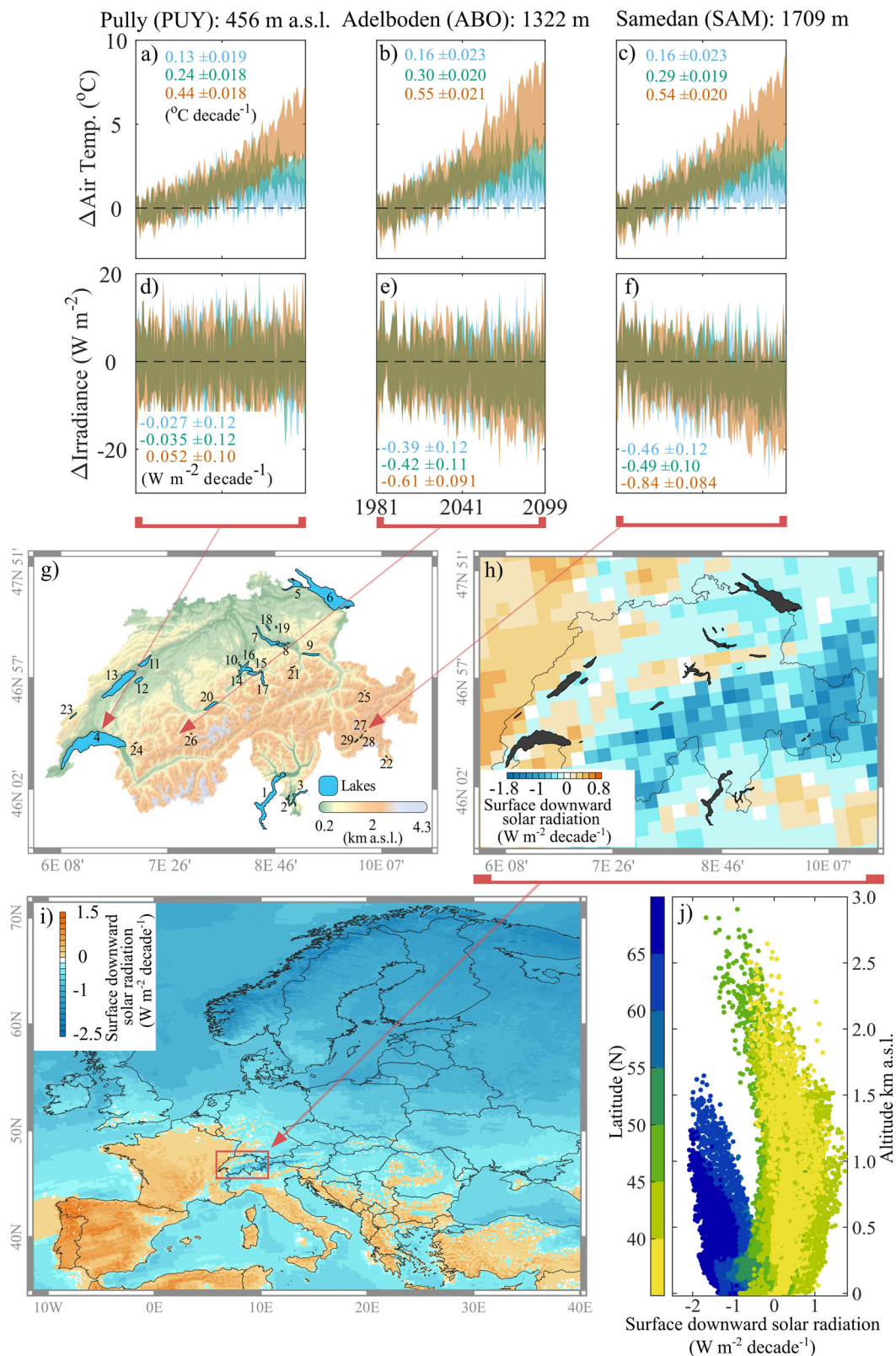


Fig. 1 Time series and trend maps of projected climate from 1981 to 2099. Temperature **a–c** and surface downward solar radiation **d–f** shown at local scale (downscaled RCM simulations). Shaded areas show the full range of annual means relative to a 1981–2010 base period for all models under scenarios RCP8.5 (orange; 17 models), RCP4.5 (green; 7 models) and RCP2.6 (blue; 7 models) with ensemble mean linear trends given for each graph. For other atmospheric forcing variables see Supplementary Fig. 2. Topography of Switzerland **g** with 29 lakes (numbered by altitude, see Table 1 for details) modelled using the Simstrat physical lake model (also in **h**). Decadal model median trend in surface downward solar radiation (RCP8.5) from 17 regional climate models for **h** Switzerland and **i** Europe, together with **j** regional European altitude vs. latitude dependent trends (10W to 40E, 35N to 70N). Maps created with QGIS v3.4, geographical data obtained for topography from www.gadm.org version 2.8, country boundaries www.naturalearthdata.com version 3.1.0, and lakes www.diva-gis.org/datadown.

Table 1 Properties of the lakes included in the present study with lakes ranked according to increasing altitude (first column) and volume (second column).

# Rank		Lake	Area	Altitude	Volume	Depth	Mixing regime		Trophic	Station
Altitude	Volume		(km ²)	(m a.s.l.)	(km ³)	(m)	1982-2010	2071-2099	State	
1	27	L. Maggiore	212.51	193	37	372	Monomictic	Monomictic	Oligotrophic	OTL
2	18	Lower L. Lugano	20	271	1.14	95	Monomictic	Monomictic	Eutrophic	LUG
3	24	Upper L. Lugano	27.3	271	4.69	288	Monomictic	Monomictic	Eutrophic	LUG
4	29	L. Geneva	582.21	372	89	309	Monomictic	Monomictic	Mesotrophic	PUY
5	16	Lower L. Constance	26.59	395	0.8	47	Monomictic	Monomictic	Mesotrophic	GUT
6	28	Upper L. Constance	481.72	395	47.6	253	Monomictic	Monomictic	Mesotrophic	GUT
7	21	Lower L. Zürich	66.6	406	3.36	136	Monomictic	Monomictic	Mesotrophic	WAE
8	14	Upper L. Zürich	20.3	406	0.47	45	Monomictic	Monomictic	Mesotrophic	WAE
9	19	Walensee	24.14	419	2.5	151	Monomictic	Monomictic	Oligotrophic	GLA
10	1	Rotsee	0.47	419	0.0038	16	Monomictic	Monomictic	Eutrophic	LUZ
11	17	L. Biel	39.3	429	1.12	73	Monomictic	Monomictic	Eutrophic	NEU
12	15	L. Murten	23	429	0.55	45	Monomictic	Monomictic	Mesotrophic	NEU
13	26	L. Neuchâtel	217.9	429	13.77	154	Monomictic	Monomictic	Mesotrophic	NEU
14	8	L. Alpnach	4.76	434	0.1	34	Dimictic	Monomictic	Oligotrophic	LUZ
15	23	L. Lucerne, Gersauer Becken	30.27	434	4.41	214	Monomictic	Monomictic	Oligotrophic	ALT
16	22	L. Lucerne, Kreuztrichter	58.92	434	4.35	151	Monomictic	Monomictic	Oligotrophic	LUZ
17	20	L. Lucerne, Urnersee	22	434	3.16	200	Monomictic	Monomictic	Oligotrophic	ALT
18	13	Greifensee	8.45	435	0.15	33	Monomictic	Monomictic	Eutrophic	SMA
19	7	Pfäffikersee	3.2	537	0.059	36	Dimictic	Dimictic/Monomictic	Mesotrophic	SMA
20	25	L. Brienz	29.8	564	5.17	260	Monomictic	Monomictic	Oligotrophic	INT
21	6	Klöntalersee	3.3	848	0.056	45	Dimictic	Monomictic	Mesotrophic	GLA
22	9	Lago di Poschiavo	1.98	962	0.12	85	Monomictic	Monomictic	Oligotrophic	ROB
23	12	Lac de Joux	8.77	1004	0.145	32	Dimictic	Dimictic/Monomictic	Oligotrophic	CHB:FRE
24	5	Lac de l'Hongrin	1.6	1250	0.0532	105	Monomictic	Monomictic	Oligotrophic	CHD:MLS
25	2	L. Davos	0.59	1558	0.0156	54	Dimictic	Monomictic	Oligotrophic	DAV
26	4	Oeschinensee	1.16	1578	0.0402	55	Monomictic	Monomictic	Eutrophic	ABO
27	3	L. St. Moritz	0.78	1768	0.02	44	Dimictic	Dimictic	Mesotrophic	SAM
28	11	L. Silvaplana	2.71	1791	0.14	78	Dimictic	Dimictic/Monomictic	Oligotrophic	SIA:SAM
29	10	L. Sils	4.11	1797	0.137	71	Dimictic	Dimictic/Monomictic	Oligotrophic	SIA:SAM

The dominant mixing regimes, defined as the regime occurring in the majority of simulated years, are given for the reference (1982–2010) and future (2071–2099) periods, bold text indicates a regime shift. Multiple regimes indicate different regimes for individual RCPs. Meteorological stations used for RCM downscaling are listed at far right. Multiple stations were combined due to missing data for individual stations (see Supporting Information).

stilling in central and northern Europe²⁴. Trends are also projected for some other atmospheric variables used in the forcing of the Simstrat model (Supplementary Fig. 2), but their effects on lake temperatures are comparably small as discussed in the following paragraph.

Lake surface temperatures vary in equilibrium with atmospheric forcing, typically increasing by $\sim 0.8^\circ\text{C}$ for a 1.0°C change in air temperature, by $\sim 0.4^\circ\text{C}$ for a 10 W m^{-2} change in surface downward solar radiation, by 0.1°C for a 0.1 m s^{-1} decrease in wind speed and by 0.1°C for a 1% increase in relative humidity⁴¹. These responses are, however, modulated by lake characteristics and mixing conditions. The projected forcing trends (Fig. 1a–f) therefore imply that for RCP8.5, air temperature trends would cause high altitude lakes to warm $\sim 0.1^\circ\text{C decade}^{-1}$ faster than low altitude lakes. The projected decrease in surface downward solar radiation, however, would reduce this warming rate by $\sim 0.035^\circ\text{C decade}^{-1}$. Projected trends in wind speed (Supplementary Fig. 2a–c) suggest a surface warming at high altitude of $\sim 0.008^\circ\text{C decade}^{-1}$ and relative humidity trends (Supplementary Fig. 2g–i) a cooling by ~ 0.02 (mid to low altitude) to ~ 0.008 (high altitude) $^\circ\text{C decade}^{-1}$, respectively. Precipitation is only used in Simstrat for the calculation of the snow cover on ice, which then affects ice growth and melting, and the projected precipitation trends will not have a relevant impact on this process. In summary, the air temperature and solar radiation trends have the largest impact on lake temperatures, and the trends of the other atmospheric variables are therefore not discussed further in this manuscript.

Changes in lake temperature are driven by heat fluxes between air and water, and these fluxes depend on meteorological conditions and lake surface temperatures^{41,42}. Average annual heat fluxes among Swiss lakes display an altitude-dependent

change in the response to climate change, strongest for RCP8.5 and weakest for RCP2.6 (Fig. 2). The effect is strongest in mid- to high-altitude lakes (from $\sim 800\text{ m a.s.l.}$), where surface downward solar radiation (H_S) and uptake (H_A) as well as emission (H_W) of infrared longwave radiation change substantially. The heat-flux trends primarily arise due to the reduced duration of lake ice cover (Fig. 3e). As ice cover recedes, lakes absorb more heat in the form of incoming longwave radiation (H_A) and surface downward solar radiation (H_S). These changes also mean increased heat loss by latent heat flux (H_E) and outgoing longwave radiation (H_W). Altitudinal gradients in air temperature and surface downward solar radiation forcing for different RCMs, combined with the large heat flux modification due to loss of lake ice, create a complex altitude-dependence in air-water heat flux variation. Finally, despite the negative trend in solar radiation at high altitudes in the atmosphere (Fig. 1), the net annual absorbed shortwave solar radiation is projected to increase for high altitude lakes due to the loss of ice (Fig. 2). Using the relationship above, the increased absorption of surface downward solar radiation due to loss of ice cover under RCP8.5 at 1700 m a.s.l. ($\sim 1.98\text{ W m}^{-2}\text{ decade}^{-1}$) leads to an increase in lake surface temperature by $\sim 0.079^\circ\text{C decade}^{-1}$.

Climate change impact on the thermal structure of lakes. The variation in the projected impacts of climate change on lake properties including thermal structure, ice and stratification results from: (i) the projected greenhouse gas concentration trajectories (RCP climate assumptions); (ii) the variation of projected atmospheric changes by the climate model chains for a given RCP; and (iii) on individual lake characteristics and how they modulate lake response to forcing scenarios.

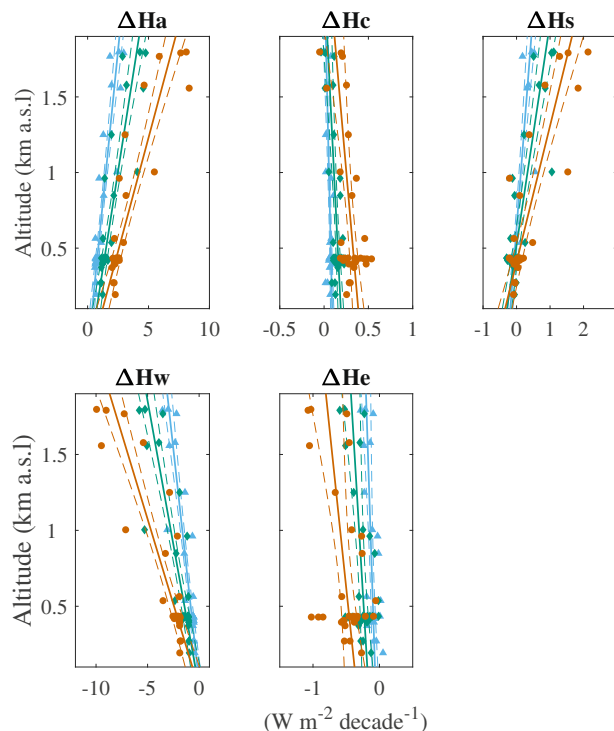


Fig. 2 Altitudinal variation in projected trends of lakes surface heat fluxes during the twenty-first century. Heat fluxes consist of uptake (H_A) and emission (H_W) of infrared longwave radiation, evaporation/condensation (H_E), sensible heat flux (H_C) and uptake of surface downward solar radiation (H_S). Positive values indicate heat uptake and negative values indicate heat loss by the lake. Data points represent the trend for each lake obtained from regression analysis of annual (1982–2099) and scenario-specific means (17 RCP8.5 orange circles, 7 RCP2.6 blue triangles, 7 RCP4.5 green diamonds). Linear regressions (solid lines) are shown with simultaneous prediction bounds for the fitted function (dashed lines, 95% confidence level), for regression coefficients and statistics see Supplementary Table 1.

For lake surface temperatures in the late twenty-first century, the RCPs are clearly the most important driver of change (Figs. 3a and 4a and Supplementary Fig. 3a–c). The average projected lake surface temperature warming compared to the reference period (average of 29 lakes in Figs. 3a and 4a) is 3.3 °C (standard deviation, SD: 0.28 °C) for RCP8.5, 1.7 °C (SD: 0.16 °C) for RCP4.5 and 0.9 °C (SD: 0.11 °C) for RCP2.6. The standard deviations given here are a measure for the individual lake response. In comparison, the variation induced by the climate models is measured with the standard deviations of all model runs for each individual lake. These are on average 0.57 °C for RCP8.5, 0.35 °C for RCP4.5 and 0.27 °C for RCP2.6, indicating that the variance induced by the climate models is about twice as large as the variation between individual lakes. A slight altitudinal difference exists (Fig. 3a and Supplementary Fig. 3c) with RCP8.5 causing an average lake surface temperature increase of 3.26 °C (SD: 0.31 °C) for high altitude lakes (>1600 m a.s.l., #27–29), 3.58 °C (SD: 0.33 °C) for mid altitude lakes (800–1600 m a.s.l., #21–26), and 3.29 °C (SD: 0.23 °C) for low altitude lakes (400–800 m a.s.l., #1–20).

Lake bottom temperatures are projected to warm at slower rates, estimated (average of 29 lakes in Figs. 3b and 4b) as 1.6 °C (SD: 0.87 °C) for RCP8.5, 0.93 °C (SD: 0.59 °C) for RCP4.5 and 0.48 °C (SD: 0.37 °C) for RCP2.6. For bottom temperatures, the variation between lakes is larger than that induced by the climate models for individual lakes, which amounts to 0.39 °C for

RCP8.5, 0.32 °C for RCP4.5 and 0.25 °C for RCP2.6. Remarkably, all emission scenarios result in lower bottom-water warming rates in smaller lakes (<0.15 km³ and <8.5 km² #10, 14, 18, 19, 21–29; with RCP8.5 modelled median changes from 0.06 to 2.10 °C, Fig. 4b). The reason for this is that despite climate change, the cooling phase in fall and winter will remain strong enough to extract the amount of heat accumulated in summer, and cool the entire lake down toward the temperature of maximum density of ~4 °C. The lake bottom temperature is thus reset every winter independent of the exact meteorological conditions. This effect is strongest at high altitude lakes, resulting in diminished bottom temperature warming rate at high altitudes. For RCP8.5 the average projected deep water temperature increase is 0.18 °C (SD: 0.10 °C) for high altitude lakes, 1.02 °C (SD: 0.71 °C) for mid altitude lakes and 2.03 °C (SD: 0.6 °C) for low altitude lakes (Fig. 3b and Supplementary Fig. 3f).

Future stratification duration in lakes. Our model results suggest that differential warming of surface and deep waters can influence the strength and duration of a given lake's stratified period. Results show substantial changes in the durations of summer and winter stratification (Fig. 3c, d). For dimictic lakes, the estimated inverse stratification duration for all lakes (average of 14 lakes, Figs. 3d and 4d) decreases by 30 days (SD: 28 days) for RCP8.5, by 18 days (SD: 13 days) for RCP4.5 and by 13 days (SD: 8 days) for RCP2.6. The estimated duration of summer stratification (average of 29 lakes in Figs. 3c and 4c) increases by 30 days (SD: 16 days) for RCP8.5, by 15 days (SD: 12 days) for RCP4.5 and by 9 days (SD: 9 days) for RCP2.6. RCP8.5 resulted in the largest changes in summer stratification with an average increase of 50 days (SD: 5 days) for high-altitude lakes (>1600 m a.s.l., #27–29), 49 days (SD: 14 days) for mid-altitude lakes (800–1600 m a.s.l., #21–26) and 22 days (SD: 9 days) for low-altitude lakes (400–800 m a.s.l., #1–20). The corresponding values for RCP2.6 are 13 days (SD: 2 days) for high-altitude lakes, 16 days (SD: 9 days) for mid-altitude lakes and 7 days (SD: 9 days) for low-altitude lakes. Estimates of the duration of winter stratification show similar altitude-dependence, where high-altitude lakes exhibit the largest decrease (Fig. 3d). RCP8.5 results in an average decrease in inverse stratification of 73 days (SD: 14 days) at high altitudes, 22 days (SD: 19 days) at mid altitudes and 14 days (SD: 15 days) at low altitudes. The corresponding values for RCP2.6 are 21 days (SD: 2 days), 12 days (SD: 9 days) and 6 days (SD: 1 day). Projected changes in summer stratification also depend on lake size (Fig. 4c), with smaller lakes (<0.5 km³) changing faster than larger lakes (>0.5 km³), which is in line with the slower bottom temperature changes in these lakes. There is no clear size dependence of the projected trends in inverse stratification (Fig. 4d).

Climate impact on ice cover duration. During the twentieth century, ice cover for larger and deeper lakes on the Swiss plateau (between 400 and 700 m a.s.l.) drastically diminished to a point of near disappearance⁴³. Model estimates for the twenty-first century indicate that persistent ice cover only develops on small, mid- to high-altitude lakes. These lakes experience shorter ice-cover duration (from #14 to 29; Fig. 3e). The ice cover duration (average of 12 lakes, Figs. 3e and 4e) is projected to decrease by 54 days (SD: 35 days) for RCP8.5, 34 days (SD: 18 days) for RCP4.5 and 18 days (SD: 7 days) for RCP2.6 in the late twenty-first century compared to the reference period.

As for inverse stratification, the RCP8.5 scenario has the most severe impacts on ice cover for lakes at high altitudes. The average decrease of ice cover duration under RCP8.5 is 85 days (SD: 24 days) at high altitudes, 44 days (SD: 39 days) at mid altitudes

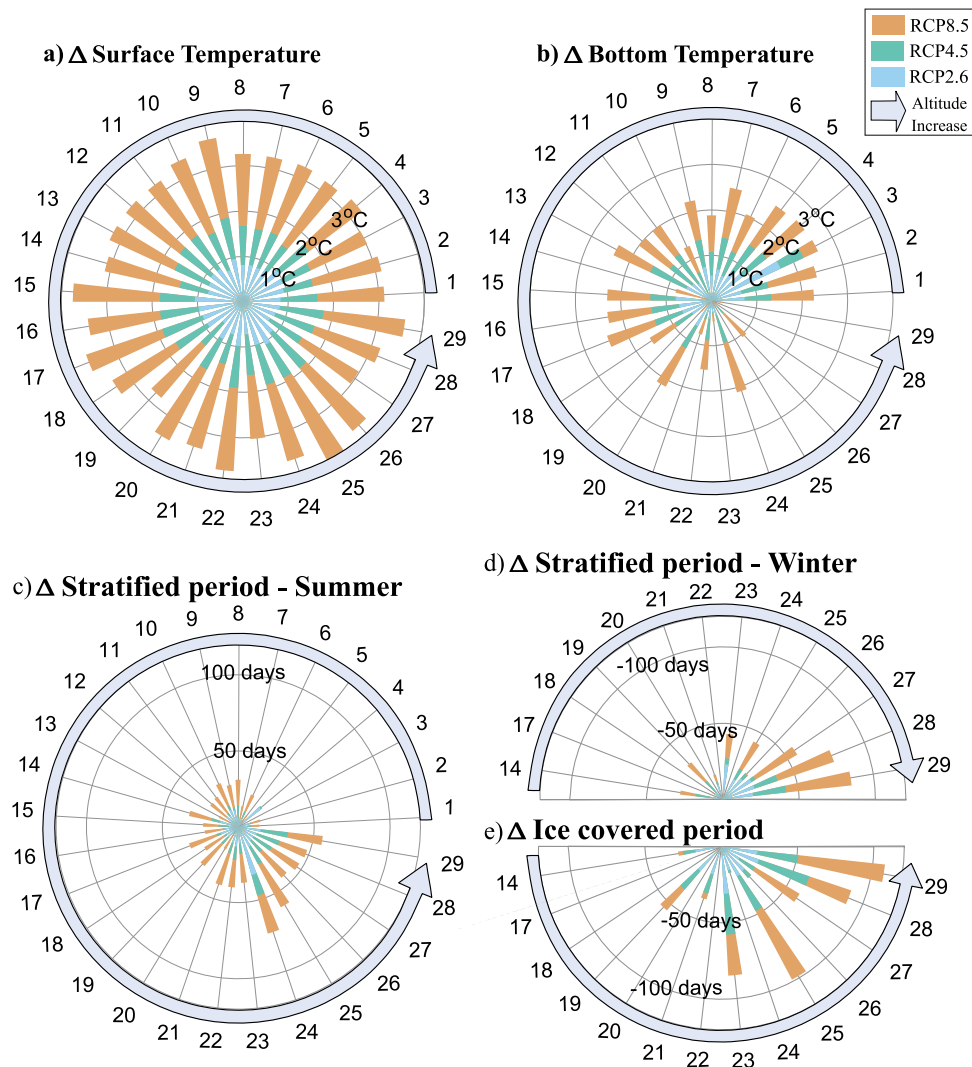


Fig. 3 Median changes in projected lake thermal properties of lakes from the reference period (1982–2010) to the late twenty-first century (2071–2099) under three RCP scenarios. For **a** lake surface temperature (at 1 m depth), **b** bottom temperatures (1 m above lake bottom), **c** duration of summer stratification, **d** duration of winter stratification and **e** duration of ice cover for scenario RCP8.5 (orange), RCP4.5 (green) and RCP2.6 (blue). The circular arrows indicate lakes ordered by altitude, from the lowest at 193 m. a.s.l. (# 1) to the highest at 1797 m a.s.l. (# 29). For lake details see Table 1.

and 41 days (SD: 18 days) at low altitudes. The corresponding values for RCP2.6 are 20 days (SD: 6 days), 18 days (SD: 9 days) and 17 days (SD: 4 days). Even though the rate of change is faster at higher altitudes, lower altitude lakes risk complete loss of ice cover. Of the three lakes that are projected to completely lose ice cover during late twenty-first century (#14 with RCP8.5, #22 with all RCPs, and #24 with RCP4.5 and RCP8.5), one resides at mid-altitude and two at low altitude. Lake volume cannot be linked to ice loss (Fig. 4e), since only the smaller lakes in this study are ice-covered in winter. Loss of ice leads to seasonal increased warming mainly in spring, with consequences for stratification duration and mixing regimes as discussed below.

Changes in lake mixing regimes. Changes in the thermal structure of lakes also modify mixing regimes. For example, a dimictic lake that presently experiences seasonal ice-cover will first lose ice cover under climate warming. This subsequently prevents winter stratification and shifts the lake over to a monomictic state. Depending on its inherent tendency to undergo complete mixing, which is a function of its morphology and exposure to wind, a lake may either remain a warm monomictic lake or further shift to an oligomictic or meromictic state with

additional warming. Table 1 and Fig. 5 show this shift in mixing regime along an altitudinal gradient for four typical lakes. High altitude lakes such as Lake St. Moritz (#27, 1768 m a.s.l., Fig. 5b) are projected to remain dimictic under all climate scenarios although with reduced duration of winter stratification and ice cover. This loss of ice will cause a greater increase in early summer lake surface temperatures and duration of summer stratification relative to that estimated from air temperature trends alone. Mid altitude lakes, such as Lac de Joux (#23, 1004 m a.s.l., Fig. 5c) or Klöntalersee (#21, 848 m a.s.l., Fig. 5d), are projected to partially or completely shift from dimictic to monomictic under some climate scenarios. This shift clearly depends on greenhouse gas concentration trajectories. The model indicates seven out of the eight dimictic lakes will shift from predominantly dimictic to primarily monomictic regimes during late twenty-first century under RCP8.5. Only three lakes make this projected transition under RCP2.6 and five make it under RCP4.5. The larger, low altitude lakes that already exhibit monomictic regimes will remain in their present states (Table 1).

The present study focuses on shifts from dimictic to monomictic mixing regimes. Due to lack of modelled instances, we did not include a detailed analysis of shifts among deep lakes

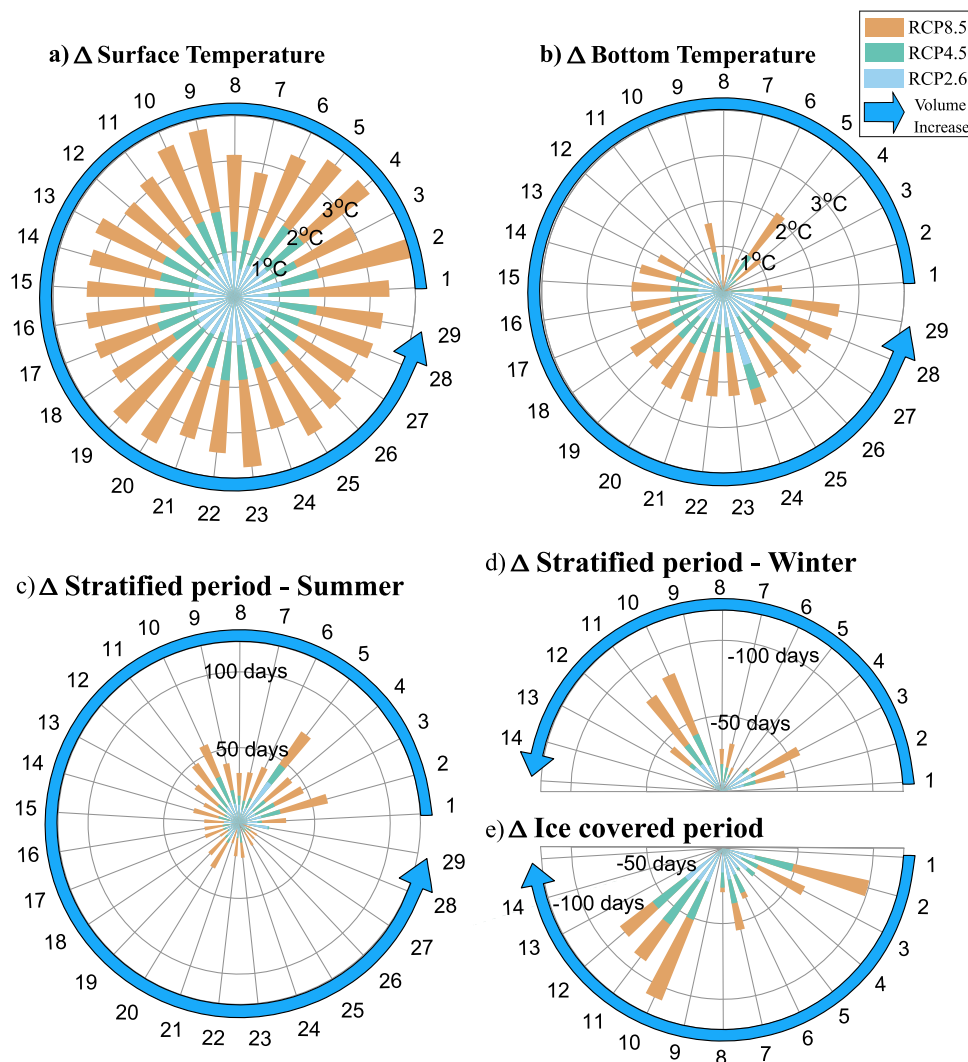


Fig. 4 Median changes in projected lake thermal properties of lakes from the reference period (1982–2010) to the late twenty-first century (2071–2099) under three RCP scenarios. Changes in **a** lake surface temperature (at 1 m depth) and **b** bottom temperatures (1 m above lake bottom), **c** duration of summer stratification, **d** duration of winter stratification and **e** duration of ice cover for scenario RCP8.5 (orange), RCP4.5 (green) and RCP2.6 (blue). Lakes are ordered by volume as denoted by the circular arrows from the smallest (#1; 0.003 km³) to the largest (#29; 89 km³). For lake details see Table 1.

from monomictic to oligomictic states or the frequency of deep mixing events among oligomictic lakes. Our results generally show that mixing regimes will shift at mid altitudes and that this shift will be larger under scenarios of higher greenhouse gas concentration trajectories (Fig. 5a). Our study suggests that the global distribution of lake thermal regions will not only shift across latitudes¹⁰ but also across altitudinal gradients. This shift is likely to obscure historical definitions of lake mixing regimes based on altitude and latitude² especially under RCP8.5. New mixing regime criteria should also consider the effects of water clarity and bathymetry recorded by this and other studies^{44,45}.

By regulating heat storage, mixing regimes are important modulators of climate impacts on lakes¹⁸. A shift from a dimictic to a warm monomictic regime increases the heat storage potential of lakes which do not cool below 4 °C. A reduced frequency and/or intensity of deep water renewal can cause hypoxia or anoxia⁴⁶ and thereby increase deep water phosphorus content⁴⁷. Reduced oxygen availability can severely reduce the habitat for higher life forms. Along with temperature increases, these may especially affect cold water fish, who face elevated temperatures from above and diminished oxygen concentrations below^{6,48}. Shifts in mixing

regime with climate change are one of the most fundamental changes that can take place in lakes. The present study outlines an important altitude dependence of these shifts, which appear most pronounced for mid altitude lakes.

Methods

Climate forcing. In this study, we use RCM simulations from EURO-CORDEX⁴⁹. The RCMs cover the European region and are forced along their boundaries using information from GCMs (Supplementary Fig. 1) for the period 1981–2099 for three different future climate scenarios. Within the RCM domain, the climate is allowed to evolve freely and includes variables for formation and breakdown of terrestrial snow and ice.

The climate data⁵⁰ used to model lake responses in this study were developed under the Swiss climate scenarios framework, CH2018 (ref. 32). In this framework, RCM simulations were statistically downscaled from the model grid to local (station) scales and aligned to atmospheric observations through non-parametric empirical quantile mapping to remove RCM biases^{32,51–54}. To do this, a day-of-year dependent correction function was created by relating the statistical distribution of the observed station data to the overlying model grid cell during the calibration period 1981–2010. The correction function was then applied to the entire simulated period⁵¹, implicitly removing the RCM biases^{52,53} and linking the grid scale with the local scale⁵⁴.

Here, we use daily data for mean air temp (tas), precipitation (pr), global radiation (rsds), relative humidity (hurs) and wind speed (sfcwind) covering the

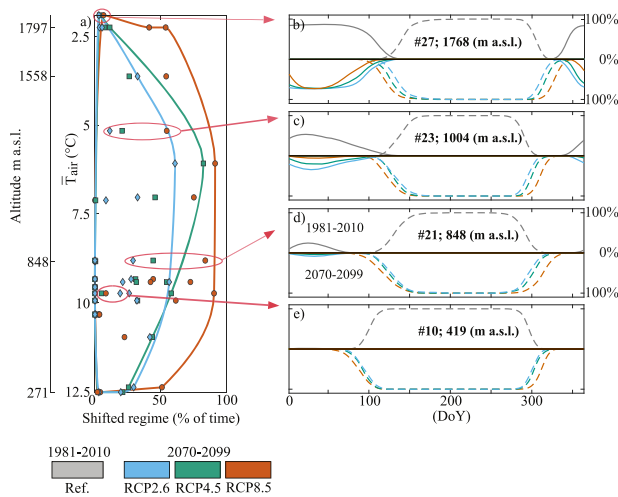


Fig. 5 Altitude-dependent changes in stratification regime for three RCP scenarios. **a** Ensemble mean (using 17 climate models for RCP8.5, and 7 models for RCP4.5 and RCP2.6) percentage of years (from 2011 to 2099) with different stratification regime relative to the mean regime during the reference period (1982–2010), where 100% indicates a shift from dimictic to annually persistent monomictic. The y-axis shows the mean air temperature in the reference period for each lake forcing station and indicates altitude for four lakes (not to scale). Smoothed lines encompass all 29 lakes under each scenario while symbols represent individual lakes (RCP2.6 blue diamonds, RCP4.5 green squares, RCP8.5 orange circles). **b–e** Percentage of occurrence of inversed winter (solid line) and summer (dashed) stratification on each day of the year (DoY) for four lakes spanning an altitude range from 419 to 1768 m a.s.l. Values are averaged over 17 or 7 climate models and 28 years for the reference (top grey) and future (bottom coloured) periods; a value of 100% means that stratification is present in all model runs and each of the 28 years on that specific day of the year. The lines are smoothed with a 10-day running mean.

period 1981–2099 from 17 RCM simulations and 3 climate scenarios downscaled to Swiss meteorological stations maintained by MeteoSwiss (Swiss Federal Office of Meteorology and Climatology). The Supplementary Table 2 lists station details, and the pairing of meteorological stations with individual lakes is given in Table 1. Using downscaled RCM data at meteorological stations ensures consistency and representativeness for the lake model, which was calibrated with observations from the stations. For four lakes (# 23, 24, 28, 29), some of the downscaled atmospheric variables were not available at the closest station. In these cases, data were combined from two nearby stations (multiple stations, Table 1). To maintain consistency, measured atmospheric variables used in the calibration were combined in the same manner. Air temperature was adjusted for station altitude differences as -0.56°C for every 100 m increase in altitude (known gradient for Switzerland²⁸).

Three RCPs (RCP2.6, RCP4.5, and RCP8.5) were used for the twenty-first century climate projections (Supplementary Fig. 1). Model simulations were made using two different spatial resolutions, EUR-11 ($0.11^{\circ}/\sim 12$ km) and EUR-44 ($0.44^{\circ}/\sim 50$ km). To visualize regional differences in Europe (Fig. 1i, j), we constructed an ensemble median dataset for each RCP using the RCMs in Supplementary Fig. 1. EUR-11 and EUR-44 simulations were combined according to Eq. (1) to include information from all models while retaining high-resolution features of the EUR-11 simulations (CH2018, Ch. 4.2.2)³².

$$\Phi_{ik} = Q(\bar{\Psi}_i^1, \dots, \bar{\Psi}_i^N, \phi_i^1, \dots, \phi_i^M) + Q(\bar{\Psi}_{ik}^1, \dots, \bar{\Psi}_{ik}^N) \quad (1)$$

where

$$\bar{\Psi}_{ik}^n = \Psi_k^n - \bar{\Psi}_{ik}^n \quad (2)$$

The ensemble median Φ is provided on the EUR-11 grid and combines N model simulations originally on the EUR-11 (Ψ) grid and M model simulations originally on the EUR-44 (ϕ) grid. N and M vary depending on climate scenario (see Supplementary Fig. 1). Overbars indicate regridded data, while k and i indicate whether the data was originally derived from the EUR-11 or EUR-44 grid, respectively. The term ik indicates the use of information from both resolutions. First, the EUR-11 simulations were regridded to the EUR-44 grid ($\bar{\Psi}_i^n$) using a bilinear distance weighting. The median (Q) was calculated for all simulations on the EUR-44 grid, and then regridded to EUR-11 resolution as indicated by the first term on the right-hand side of Eq. (1). Second, in order to retain the

high-resolution features, $\bar{\Psi}_i^n$ was regridded back to the original EUR-11 grid. This resulted in low resolution versions ($\bar{\Psi}_{ik}^n$) of the high-resolution simulations (Ψ_k^n) for the EUR-11 grid. The median was then calculated from the anomalies in the EUR-11 simulations relative to the low-resolution version (Eq. (2)). These were added to the combined median estimate from EUR-44 and EUR-11.

The physical lake model Simstrat requires air temperature, wind speed, precipitation, vapour pressure, downward shortwave solar and either downward longwave radiation or fractional cloud cover as forcing variables. These variables were obtained from the CH2018 framework downscaled scenarios, yet two variables were not available, downward longwave radiation and fractional cloud cover. Therefore, shortwave solar radiation was used to estimate fractional cloud cover, c , which was then used by Simstrat to calculate downward longwave radiation. The fractional cloud cover was estimated as

$$c = \frac{P_{sf}}{k_{cld} - k_{clr}} + 1 - \frac{k_{cld}}{k_{cld} - k_{clr}} \quad (3)$$

where P_{sf} is the potential solar fraction defined as $P_{sf} = I_s / C_{ssr}$. In this expression, I_s is observed (or downscaled RCM) shortwave solar irradiance and C_{ssr} is clear sky solar radiation. Equation (3) linearly interpolates cloud cover between 1.0 (P_{sf} equal to the clearness index for complete cloud cover, k_{cld}) and 0.0 (P_{sf} equal to the clear sky index, k_{clr}). These two indices depend on location⁵⁵ and were obtained during the calibration period (lake dependent; Supplementary Table 3) by minimizing the root mean square difference between observed and modelled c at each meteorological station. Indices are given in 0.05 increments. C_{ssr} is calculated using the Lake Heat Flux Analyzer⁵⁶. The statistical distributions of the estimates for c are compared to observations during the calibration period (Supplementary Figure 4). Supplementary Table 2 lists values for k .

Lake model. The physical deterministic one-dimensional lake model Simstrat³⁰ (v. 2.1.2) includes surface lake ice³¹, constant lake dependent geothermal heat flux and a k - ϵ turbulence closure scheme driven by wind and internal waves. The recently added ice and snow module³¹ based on previous work^{57–59} generates estimates for snow pack, which can delay the ice melting²⁷ by isolating the ice-cover. The version of the model used here did not include inflows and outflows, and thus future cooling effects of increased meltwater inflows, drainage area processes or anthropogenic discharge and thermal usage that could potentially modify lake temperatures^{28,34} outside of historical parameter calibration. Visible light attenuation, geothermal heat flux, bathymetry, initial conditions, air pressure and latitude were all lake dependent.

The lake model was calibrated with in situ data for 27 of the 29 lakes (no observations available for lakes #24 and 25) with four model parameters (Supplementary Table 3) using PEST (model-independent parameter estimation software; <http://pesthomedpage.org>). Parameters selected for calibration and the rationale for their selection have been described previously³¹. The remaining model parameters are set to standard values. To match the temporal resolution of climate projections, calibrations used daily averaged measurements from nearby meteorological stations (Table 1). To check the sensitivity of the daily temporal resolution of the forcing data, Simstrat was additionally calibrated using hourly instead of daily averaged forcing. This gave similar model performance for both time increments (Supplementary Fig. 5).

Among available one-dimensional lake models, Simstrat has been shown to generate accurate results for both surface and bottom waters in deep lakes⁶⁰. The original Simstrat model has a tendency to overestimate the internal wave energy in winter and thus the occurrence of mixing events in deep lakes. This can be avoided by filtering out high-frequency wind events (removing wind events shorter than $\sim 1/4$ the first internal wave mode period)⁶¹ or by using seasonally varying parameterization for α^7 . In order to limit the number of parameters and manage computational resources, the model used seasonally varying α only for lakes deeper than 150 m, an approach which adequately improved model results (Supplementary Table 3). The point where α_w (winter) changes to α_s (summer) can be assigned to a specific day of the year⁷, but this transition is expected to change with changing climate. The model therefore switches α_s to α_w once thermal stratification disappears, i.e., if the maximum Brunt–Väisälä frequency (N^2) during a time step drops below a set limit. N^2 is equal to $-g/\rho^*dp/dz$ where g is gravitational acceleration, ρ is water density, and z is the vertical axis pointing upward. The N^2 limit depends on the grid resolution of the model (0.5 m). N^2 was set to $2 \times 10^{-4} \text{ s}^{-2}$ based on temporal evaluation of maximum values for N^2 during the reference period (1982–2010). Using real measured atmospheric forcing of Lake Geneva between 1981 and 2011 (31 years), the seasonal α method resulted in 16 modelled overturn events compared with 15 observed events (detected in monthly CTD profiles).

Calculations. According to the conventions of the CH2018 climate analyses, a 30-year reference time period from 1981 to 2010 was used and compared to the late twenty-first century period from 2070 to 2099. However, since the first simulation year could include spin-up effects, we dropped it from the analysis and used 1982 to 2010 as the reference period instead. To be consistent, the first year was also dropped for the late twenty-first century, and averages were calculated from 2071 to 2099. The approximate thirty years' classical time frame aims at removing random effects due to interannual variability³³.

All calculations were performed in MATLAB R 2017b and statistical properties such as trends, means, medians and variances were calculated first for each individual RCM and then for each RCP. For example, in Fig. 3a, the median surface temperature change from the reference period to late twenty-first century was calculated as follows. First, annual means (temperatures) and annual sums (stratification, ice) for each RCM simulation were obtained. Second, differences between the two periods were calculated for each RCM simulation. Third, medians, means and variances across the models (7 models in RCP2.6 and RCP4.5, and 17 for RCP8.5) of this difference were calculated (Figs. 3 and 4 and Supplementary Fig. 6).

A lake is considered to be stratified if the temperature difference (ΔT) between the surface water (10 m mean) and the bottom water (lowest point) exceeds 1°C^{62} . The surface mean temperature was averaged over the top 10 m to remove short-term temperature fluctuations. Lakes investigated in this study are all deep (Table 1), and water exchange between surface and bottom is limited when a significant density gradient develops. In summer $\Delta T > 1^\circ\text{C}$ results in stable stratification, while in winter $\Delta T < -1$ describes an inverse stable stratification. Multiple stratified periods in both summer and winter, separated with short gaps (<15 days) due to strong short-term mixing events, were merged prior to estimating the total annual stratification duration.

Future and past mixing regimes were classified as either warm monomictic (overturn once in winter), dimictic (overturn twice per year, in autumn and in spring) or oligomictic (irregular overturns, not occurring every year). A lake overturn is defined to have occurred if surface temperature (10 m average) becomes colder or equal to bottom temperature after a previous summer stratification (monomictic, oligomictic and dimictic lakes), or if the surface temperature becomes warmer or equal to bottom temperature following an inverse stratification (dimictic lakes).

Stratification regimes were obtained annually (Fig. 5a), and as periodic means during the reference period (1982–2010) and for the late twenty-first century (2071–2099) (Table 1 and Fig. 5b–e). A lake was first classified for each simulated year as dimictic, monomictic or meromictic (no mixing). The final classification was then defined as dimictic or monomictic, if that was the regime occurring in most years for each climate scenario, or as oligomictic, if it was classified as meromictic in most years.

Data availability

Simstrat simulation output are available in an open access repository (<https://doi.org/10.25678/0002SF>). The RCM dataset (DAILY-LOCAL) used to force Simstrat can be obtained upon request from the Swiss National Centre for Climate Services (NCCS, <https://doi.org/10.18751/Climate/Scenarios/CH2018/1.0>). The raw CORDEX data can be accessed through the Earth System Grid Federation (ESGF: <https://esgf-node.llnl.gov/projects/esgf-llnl/>).

Code availability

The one-dimensional Simstrat physical lake model can be accessed on github (<https://github.com/Eawag-AppliedSystemAnalysis/Simstrat>).

Received: 15 July 2020; Accepted: 22 January 2021;

Published online: 18 February 2021

References

- Adrian, R. et al. Lakes as sentinels of climate change. *Limnol. Oceanogr.* **54**, 2283–2297 (2009).
- Hutchinson, G. E. & Löffler, H. The thermal classification of lakes. *Proc. Natl. Acad. Sci. USA* **42**, 84–86 (1956).
- Schweifel, R., Müller, B., Boigontier, H. & Wüest, A. Global warming affects nutrient upwelling in deep lakes. *Aquat. Sci.* **81**, 50 (2019).
- Yankova, Y., Neuenschwander, S., Köster, O. & Posch, T. Abrupt stop of deep water turnover with lake warming: drastic consequences for algal primary producers. *Sci. Rep.* **7**, 13770 (2017).
- Kraemer, B. M. et al. Global patterns in lake ecosystem responses to warming based on the temperature dependence of metabolism. *Glob. Change Biol.* **23**, 1881–1890 (2017).
- Missaghi, S., Hondzo, M. & Herb, W. Prediction of lake water temperature, dissolved oxygen, and fish habitat under changing climate. *Clim. Change* **141**, 747–757 (2017).
- Schweifel, R., Gaudard, A., Wüest, A. & Bouffard, D. Effects of climate change on deepwater oxygen and winter mixing in a deep lake (Lake Geneva): comparing observational findings and modeling. *Water Resour. Res.* **52**, 8811–8826 (2016).
- Posch, T., Köster, O., Salcher, M. M. & Pernthaler, J. Harmful filamentous cyanobacteria favoured by reduced water turnover with lake warming. *Nat. Clim. Change* **2**, 809–813 (2012).
- Peeters, F., Straile, D., Lorke, A. & Livingstone, D. M. Earlier onset of the spring phytoplankton bloom in lakes of the temperate zone in a warmer climate. *Glob. Change Biol.* **13**, 1898–1909 (2007).
- Maberly, S. C. et al. Global lake thermal regions shift under climate change. *Nat. Commun.* **11**, 1232 (2020).
- Piccolroaz, S., Woolway, R. I. & Merchant, C. J. Global reconstruction of twentieth century lake surface water temperature reveals different warming trends depending on the climatic zone. *Clim. Change* **160**, 427–442 (2020).
- O'Reilly, C. M. et al. Rapid and highly variable warming of lake surface waters around the globe. *Geophys. Res. Lett.* **42**, 10773–10781 (2015).
- Sharma, S. et al. Widespread loss of lake ice around the Northern Hemisphere in a warming world. *Nat. Clim. Change* **9**, 227–231 (2019).
- Gebre, S., Boissy, T. & Alfredsen, K. Sensitivity of lake ice regimes to climate change in the Nordic region. *Cryosphere* **8**, 1589–1605 (2014).
- Dibike, Y., Prowse, T., Saloranta, T. & Ahmed, R. Response of Northern Hemisphere lake-ice cover and lake-water thermal structure patterns to a changing climate. *Hydrol. Process.* **25**, 2942–2953 (2011).
- Weyhenmeyer, G. A., Meili, M. & Livingstone, D. M. Nonlinear temperature response of lake ice breakup. *Geophys. Res. Lett.* **31**, L07203 (2004).
- Magnuson, J. J. et al. Historical trends in lake and river ice cover in the northern hemisphere. *Science* **289**, 1743–1746 (2000).
- Shatwell, T., Thiery, W. & Kirillin, G. Future projections of temperature and mixing regime of European temperate lakes. *Hydrol. Earth Syst. Sci.* **23**, 19 (2019).
- Woolway, R. I. & Merchant, C. J. Worldwide alteration of lake mixing regimes in response to climate change. *Nat. Geosci.* **12**, 271–276 (2019).
- Kraemer, B. M. et al. Morphometry and average temperature affect lake stratification responses to climate change. *Geophys. Res. Lett.* **42**, 4981–4988 (2015).
- Kirillin, G. Modeling the impact of global warming on water temperature and seasonal mixing regimes in small temperate lakes. *Boreal Environ. Res.* **15**, 279–293 (2010).
- Austin, J. A. & Colman, S. M. Lake superior summer water temperatures are increasing more rapidly than regional air temperatures: a positive ice-albedo feedback. *Geophys. Res. Lett.* **34**, L06604 (2007).
- Wang, J. et al. Temporal and spatial variability of great lakes ice cover, 1973–2010. *J. Clim.* **25**, 1318–1329 (2012).
- Woolway, R. I. et al. Northern hemisphere atmospheric stilling accelerates lake thermal responses to a warming world. *Geophys. Res. Lett.* **46**, 11983–11992 (2019).
- Schmid, M. & Köster, O. Excess warming of a Central European lake driven by solar brightening. *Water Resour. Res.* **52**, 8103–8116 (2016).
- Pepin, N. et al. Elevation-dependent warming in mountain regions of the world. *Nat. Clim. Change* **5**, 424–430 (2015).
- Ceppi, P., Scherrer, S. C., Fischer, A. M. & Appenzeller, C. Revisiting Swiss temperature trends 1959–2008. *Int. J. Climatol.* **32**, 203–213 (2012).
- Livingstone, D. M., Lotter, A. F. & Kettle, H. Altitude-dependent differences in the primary physical response of mountain lakes to climatic forcing. *Limnol. Oceanogr.* **50**, 1313–1325 (2005).
- Riffler, M., Lieberherr, G. & Wunderle, S. Lake surface water temperatures of European Alpine lakes (1989–2013) based on the Advanced Very High Resolution Radiometer (AVHRR) 1 km data set. *Earth Syst. Sci. Data* **7**, 1–17 (2015).
- Goudsmit, G.-H., Burchard, H., Peeters, F. & Wüest, A. Application of k-ε turbulence models to enclosed basins: The role of internal seiches. *J. Geophys. Res.* **107**, 3230 (2002).
- Gaudard, A., Răman Vinnă, L., Bärenbold, F., Schmid, M. & Bouffard, D. Toward an open access to high-frequency lake modeling and statistics data for scientists and practitioners—the case of Swiss lakes using Simstrat v2.1. *Geosci. Model Dev.* **12**, 3955–3974 (2019).
- CH2018. *CH2018—Climate scenarios for Switzerland*. Technical Report, National Center for Climate Services, Zürich. pp. 271 (2018).
- IPCC. *Climate Change 2013: The Physical Science Basis*. Contribution of Working Group I to the Fifth Assessment Report of the Intergovernmental Panel on Climate Change 1535 [eds. Stocker, T. F. et al.]. (Cambridge University Press, 2013).
- Răman Vinnă, L., Wüest, A., Zappa, M., Fink, G. & Bouffard, D. Tributaries affect the thermal response of lakes to climate change. *Hydrol. Earth Syst. Sci.* **22**, 31–51 (2018).
- Sommer, C. et al. Rapid glacier retreat and downwasting throughout the European Alps in the early 21st century. *Nat. Commun.* **11**, 3209 (2020).
- Christianson, K. R. & Johnson, B. M. Combined effects of early snowmelt and climate warming on mountain lake temperatures and fish energetics. *Arct. Antarct. Alp. Res.* **52**, 130–145 (2020).
- Roberts, D. C., Forrest, A. L., Sahoo, G. B., Hook, S. J. & Schladow, S. G. Snowmelt timing as a determinant of lake inflow mixing. *Water Resour. Res.* **54**, 1237–1251 (2018).

38. Christianson, K. R., Johnson, B. M. & Hooten, M. B. Compound effects of water clarity, inflow, wind and climate warming on mountain lake thermal regimes. *Aquat. Sci.* **82**, 6 (2020).
39. Mi, H., Fagherazzi, S., Qiao, G., Hong, Y. & Fichot, C. G. Climate change leads to a doubling of turbidity in a rapidly expanding Tibetan lake. *Sci. Total Environ.* **688**, 952–959 (2019).
40. Boé, J., Somot, S., Corre, L. & Nabat, P. Large discrepancies in summer climate change over Europe as projected by global and regional climate models: causes and consequences. *Clim. Dyn.* **54**, 2981–3002 (2020).
41. Schmid, M., Hunziker, S. & Wüest, A. Lake surface temperatures in a changing climate: a global sensitivity analysis. *Clim. Change* **124**, 301–315 (2014).
42. Fink, G., Schmid, M., Wahl, B., Wolf, T. & Wüest, A. Heat flux modifications related to climate-induced warming of large European lakes. *Water Resour. Res.* **50**, 2072–2085 (2014).
43. Hendricks-Franssen, H. J. & Scherrer, S. C. Freezing of lakes on the Swiss plateau in the period 1901–2006. *Int. J. Climatol.* **28**, 421–433 (2008).
44. Lewis, W. M. A revised classification of lakes based on mixing. *Can. J. Fish. Aquat. Sci.* **40**, 1779–1787 (1983).
45. Kirillin, G. & Shatwell, T. Generalized scaling of seasonal thermal stratification in lakes. *Earth Sci. Rev.* **161**, 179–190 (2016).
46. North, R. P., North, R. L., Livingstone, D. M., Köster, O. & Kipfer, R. Long-term changes in hypoxia and soluble reactive phosphorus in the hypolimnion of a large temperate lake: consequences of a climate regime shift. *Glob. Change Biol.* **20**, 811–823 (2014).
47. Ficker, H., Luger, M. & Gassner, H. From dimictic to monomictic: empirical evidence of thermal regime transitions in three deep alpine lakes in Austria induced by climate change. *Freshw. Biol.* **62**, 1335–1345 (2017).
48. Magee, M. R., McIntyre, P. B. & Wu, C. H. Modeling oxythermal stress for cool-water fishes in lakes using a cumulative dosage approach. *Can. J. Fish. Aquat. Sci.* **75**, 1303–1312 (2018).
49. Giorgi, F., Jones, C. & Asrar, G. R. Addressing climate information needs at the regional level: the CORDEX framework. *WMO Bull.* **58**, 175–183 (2009).
50. CH2018 Project Team. *CH2018—Climate Scenarios for Switzerland* (National Centre for Climate Services, 2018).
51. Feigenwinter, I. et al. *Exploring Quantile Mapping as a Tool to Produce User-Tailored Climate Scenarios for Switzerland*. Technical Report No. 270, 44 (MeteoSwiss, 2018).
52. Ivanov, M. A. & Kotlarski, S. Assessing distribution-based climate model bias correction methods over an alpine domain: added value and limitations. *Int. J. Climatol.* **37**, 2633–2653 (2017).
53. Rajczak, J., Kotlarski, S. & Schär, C. Does quantile mapping of simulated precipitation correct for biases in transition probabilities and spell lengths? *J. Clim.* **29**, 1605–1615 (2016).
54. Rajczak, J., Kotlarski, S., Salzmann, N. & Schär, C. Robust climate scenarios for sites with sparse observations: a two-step bias correction approach. *Int. J. Climatol.* **36**, 1226–1243 (2016).
55. Flerchinger, G. N., Xao, W., Marks, D., Sauer, T. J. & Yu, Q. Comparison of algorithms for incoming atmospheric long-wave radiation. *Water Resour. Res.* <https://doi.org/10.1029/2008WR007394> (2009).
56. Woolway, R. I. et al. Automated calculation of surface energy fluxes with high-frequency lake buoy data. *Environ. Model. Softw.* **70**, 191–198 (2015).
57. Leppäranta, M. *Freezing of Lakes and the Evolution of their Ice Cover* (Springer, 2014).
58. Leppäranta, M. In *The Impact of Climate Change on European Lakes* (ed. George, G.) 63–83 (Springer, 2010).
59. Saloranta, T. M. & Andersen, T. MyLake—a multi-year lake simulation model code suitable for uncertainty and sensitivity analysis simulations. *Ecol. Modell.* **207**, 45–60 (2007).
60. Perroud, M., Goyette, S., Martynov, A., Beniston, M. & Anneville, O. Simulation of multiannual thermal profiles in deep Lake Geneva: a comparison of one-dimensional lake models. *Limnol. Oceanogr.* **54**, 1574–1594 (2009).
61. Gaudard, A. et al. Optimizing the parameterization of deep mixing and internal seiches in one-dimensional hydrodynamic models: a case study with Simstrat v1.3. *Geosci. Model. Dev.* **10**, 3411–3423 (2016).
62. Foley, B., Jones, I. D., Maberly, S. C. & Rippey, B. Long-term changes in oxygen depletion in a small temperate lake: effects of climate change and eutrophication: oxygen depletion in a small lake. *Freshw. Biol.* **57**, 278–289 (2012).

Acknowledgements

This study was financially supported by the Swiss Federal Office for the Environment (FOEN) as part of the project “Hydrologische Grundlagen zum Klimawandel” (Hydro-CH2018). We thank Silje Sørland for EURO-CORDEX expertise, Adrien Gaudard for helping with the Simstrat model setup, Alfred Wüest and Hendrik Huwald for contributing to the development of the project proposal.

Author contributions

D.B. and M.S. conceived and supervised the study; L.R.V., D.B. and M.S. designed the methodology; L.R.V. performed the lake modelling, the data curation and the formal analysis; D.B. and M.S. contributed to the formal analysis; I.M. analysed the raw RCM data; data visualization was designed by L.R.V., I.M., D.B. and M.S. and implemented by L.R.V.; L.R.V. prepared the initial draft of the manuscript; D.B., I.M. and M.S. reviewed and edited the manuscript.

Competing interests

The authors declare no competing interests.

Additional information

Supplementary information The online version contains supplementary material available at <https://doi.org/10.1038/s43247-021-00106-w>.

Correspondence and requests for materials should be addressed to L.R.V. or D.B.

Peer review information Primary handling editor: Heike Langenberg.

Reprints and permission information is available at <http://www.nature.com/reprints>

Publisher's note Springer Nature remains neutral with regard to jurisdictional claims in published maps and institutional affiliations.



Open Access This article is licensed under a Creative Commons Attribution 4.0 International License, which permits use, sharing, adaptation, distribution and reproduction in any medium or format, as long as you give appropriate credit to the original author(s) and the source, provide a link to the Creative Commons license, and indicate if changes were made. The images or other third party material in this article are included in the article's Creative Commons license, unless indicated otherwise in a credit line to the material. If material is not included in the article's Creative Commons license and your intended use is not permitted by statutory regulation or exceeds the permitted use, you will need to obtain permission directly from the copyright holder. To view a copy of this license, visit <http://creativecommons.org/licenses/by/4.0/>.

© The Author(s) 2021